13th International Symposium on Turbulence and Shear Flow Phenomena (TSFP13)
Montreal, Canada, June 25–28, 2024

CHARACTERISTICS OF ACTIVE AND INACTIVE MOTIONS IN HIGH-REYNOLDS-NUMBER TURBULENT BOUNDARY LAYERS

Rahul Deshpande[1], Ricardo Vinuesa[2], Ivan Marusic[1]

[1]Department of Mechanical Engineering, The University of Melbourne, Victoria 3010, Australia
[2]FLOW, Engineering Mechanics, KTH Royal Institute of Technology, Stockholm, 10044, Sweden

ABSTRACT

Wall-scaled (attached) eddies play a significant role in the overall drag experienced in high-Reynolds-number turbulent boundary layers (TBLs). This study aims to delve into the underlying mechanisms driving this phenomenon by dissecting the active and inactive components of these attached eddies, as initially proposed by Townsend (1976). Employing a recently introduced energy-decomposition scheme, we analyze TBL datasets covering a wide range of Reynolds numbers ($Re_\tau \sim \mathcal{O}(10^3)$–$\mathcal{O}(10^6)$)). This analysis provides empirical evidence of the distinct contributions of these components to drag generation, and reveals that while active motions are responsible solely for generating Reynolds shear stresses, inactive motions are crucial for transporting streamwise momentum from the logarithmic region to the wall, thus corroborating earlier hypotheses in the literature.

INTRODUCTION & MOTIVATION

Flow over an airplane wing or over a ship hull corresponds to a turbulent boundary layer (TBL) at a very high friction Reynolds number ($Re_\tau > 10^5$; where $Re_\tau = U_\tau\delta/\nu$ with U_τ, δ and ν being the mean friction velocity, boundary layer thickness and kinematic viscosity, respectively), resulting in significant power requirements to overcome the skin-friction drag produced by the overlying TBL. Despite such economic incentives on offer, progress in understanding the flow physics responsible for this drag has been slow owing to differing governing mechanisms in low ($Re_\tau \lesssim 10^3$) and high ($Re_\tau \gtrsim 10^4$) Re_τ flows, with only the former easily realizable in a laboratory (Marusic *et al.*, 2021). While the viscous-scaled coherent motions in the near-wall region are responsible for generating drag at low Re_τ (Kim, 2011; Corke & Thomas, 2018), the energy containing self-similar motions in the log/inertial region have been shown to generate a significant portion of the total drag at Re_τ relevant to the transportation industry and several other engineering applications (Deck *et al.*, 2014; de Giovanetti *et al.*, 2016; Marusic *et al.*, 2021). The log region is also responsible for the bulk production of the turbulent kinetic energy at these high Re_τ (Marusic *et al.*, 2010; Smits *et al.*, 2011), encouraging the modelling of this region and making it an area of active research.

Of the several models proposed in the literature, the conceptual model by Townsend (1976) known as the attached eddy model (AEM), which is based on his attached eddy hypothesis, is one of the most prominent (Marusic & Monty, 2019). The AEM essentially models the kinematics in the log region of a canonical TBL flow by a hierarchy of inertia-dominated, geometrically self-similar eddying motions that extend to the wall and are randomly distributed in the flow field. These eddies have a population density inversely proportional to their height ($\mathcal{H}$), that varies between $\mathcal{O}(z_l) \lesssim \mathcal{H} \lesssim \mathcal{O}(\delta)$. Here, z_l corresponds to the lower bound of the log region ($z_l^+ \approx 2.6\sqrt{Re_\tau}$) while its viscous-scaled upper bound is generally accepted to be $0.15Re_\tau$. As per the hypothesis, such a distribution yields a logarithmic variation in the variances of the viscous-scaled wall-parallel velocity fluctuations ($\overline{u^2}^+$, $\overline{v^2}^+$), while the wall-normal velocity variance ($\overline{w^2}^+$) and the Reynolds shear stresses ($\overline{uw}^+$) tend to be a constant with the wall-normal coordinate z following:

$$\overline{u^2}^+ = B_1 - A_1 \ln\left(\frac{z}{\delta}\right), \quad \overline{v^2}^+ = B_2 - A_2 \ln\left(\frac{z}{\delta}\right), \quad \overline{w^2}^+ = B_3 \quad \text{and} \quad \overline{uw}^+ = -1, \tag{1}$$

with B_{1-3} and A_{1-2} being constants. One can find substantial empirical evidence in support of these expressions in the literature (Jimenez & Hoyas, 2008; Hultmark *et al.*, 2012; Lee & Moser, 2015; Pirozzoli *et al.*, 2021; Deshpande *et al.*, 2021). The contrasting nature of variation between ($\overline{u^2}^+$, $\overline{v^2}^+$) and ($\overline{w^2}^+$, $\overline{uw}^+$) in (1) was explained by Townsend (1976) via decomposition of the total flow at any z, in the log region, into 'active' and 'inactive' contributions. Here, the active motions correspond to the 'localized' attached eddies of height, $\mathcal{H} \sim \mathcal{O}(z)$, and they add to $\overline{u^2}(z)$, $\overline{v^2}(z)$, $\overline{w^2}(z)$ and $\overline{uw}(z)$. While, the inactive contributions come from the relatively large and tall attached eddies of height, $\mathcal{O}(z) \ll \mathcal{H} \lesssim \mathcal{O}(\delta)$, that only add to $\overline{u^2}(z)$ and $\overline{v^2}(z)$ but not to $\overline{w^2}(z)$ and $\overline{uw}(z)$. Based on the above description, the active motions can be described as the sole Reynolds shear stress producing motions in the log region (Deshpande *et al.*, 2021; Deshpande & Marusic, 2021). Interested readers can refer to these papers for further and elaborate discussions on this topic. These discussions inspire the decomposition of the attached eddy

Table 1. Details of various published multi-point datasets of canonical TBLs used in the present study. LES indicates Large Eddy Simulations, HRNBLWT indicates High Reynolds Number Boundary Layer Wind Tunnel Facility at the University of Melbourne, and SLTEST refers to the Surface Layer Turbulence and Environmental Science Test (SLTEST) facility in western Utah. Bold and underlined numbers respectively refer to the lower and upper bounds of the log region, *i.e.* $z^+ \sim 2.6\sqrt{Re_\tau}$ and $0.15Re_\tau$.

Re_τ	Facility/ Simulations	Wall ($z = 0$) sensor	log region sensor	log region range	Reference
2000	LES	-	-	$\mathbf{100} \lesssim z^+ \lesssim \underline{250}$	Eitel-Amor *et al.* (2014)
15000	HRNBLWT	hot-film	cross-wire	$\mathbf{300} \lesssim z^+ \lesssim \underline{2250}$	Talluru *et al.* (2014)
$\mathcal{O}(10^6)$	SLTEST	shear sensor	sonics	$3360 \lesssim z^+ \lesssim 41000$	Marusic & Heuer (2007)

velocity fields per the following (Panton, 2007):

$$\begin{aligned} u &= u_\mathrm{a} + u_\mathrm{ia}, \\ v &= v_\mathrm{a} + v_\mathrm{ia}, \\ w &= w_\mathrm{a}, \end{aligned} \tag{2}$$

where subscripts 'a' and 'ia' represent active and inactive contributions, respectively.

Given that the attached eddies are statistically significant in generating skin-friction drag in a high-Re_τ TBL (Deck *et al.*, 2014; de Giovanetti *et al.*, 2016; Marusic *et al.*, 2021), it is worth considering how their active and inactive components individually contribute to this dynamical process. Townsend (1976) described inactive motions as *non-local* 'swirling motions' whose "*effect on that part of the layer between the point of observation and the wall is one of slow random variation of 'mean velocity' which cause corresponding variation of wall stress.*" In other words, owing to the relatively large spatial coherence of the inactive motions compared to the active motions at any z, Townsend (1976) described the former to be influencing the velocity field at all wall heights below z, including the wall-shear stress fluctuations (via low-frequency fluctuations). This characteristic of the inactive motions was hypothesized by de Giovanetti *et al.* (2016) as the pathway through which the attached eddies contribute to the turbulent skin-friction drag. They argued that the attached eddies generate Reynolds shear stress through their active part but transport the streamwise momentum to the wall through their inactive part. This hypothesis has important implications for the future flow control schemes, but has not been tested yet due to the absence of a reliable methodology that can decompose the log region flow into its active and inactive components. To this end, the present study demonstrates the efficacy of a recently proposed decomposition methodology (Deshpande *et al.*, 2021; Deshpande & Marusic, 2021) on TBL datasets spanning a large-Re_τ range ($Re_\tau \sim 10^3$ – 10^6), thereby permitting testing of the hypothesis proposed by de Giovanetti *et al.* (2016) for the first time.

DATASETS AND METHODOLOGY

The present study considers three published, multi-point datasets from canonical TBLs (table 1). The data set at lowest Re_τ ($\sim$ 2000) is from the well-resolved large-eddy simulation (LES) of Eitel-Amor *et al.* (2014). The intermediate Re_τ ($\sim$ 15000) data was acquired in the large Melbourne wind tunnel (HRNBLWT; (Talluru *et al.*, 2014)) using hot-film sensors (on the wall) and cross-wire sensors. While the data set at highest Re_τ ($\sim \mathcal{O}(10^6)$) was acquired at the atmospheric surface layer facility (SLTEST) in neutrally-buoyant conditions, using a combination of sonic anemometers and a unique wall-shear stress sensor (Marusic & Heuer, 2007). Hence, each of these datasets provide access to the time-series of the instantaneous wall-shear-stress fluctuations (τ_w) acquired/computed synchronously with the $\{u,w\}$ fluctuations in the log region, by a probe placed vertically above the wall-sensor.

Notable differences between these data sets, however, are in the length/duration of the available time series and the multi-point nature of data acquisition. In case of the HRNBLWT data, τ_w was acquired simultaneously with a cross-wire probe, which was traversed across the canonical TBL to measure long time series of u, w at logarithmically spaced z-locations. As a consequence, the u, w-fluctuations acquired at each z-location are statistically independent from one another. Further, the time series data from the HRNBLWT was acquired for a sufficiently long sampling time ($t_\mathrm{samp} \sim 360$ s), such that $t_\mathrm{samp}U_\infty/\delta \gtrsim 30000$, which ensures converged large-scale spectral features. In contrast, the duration of the available time series from the LES and SLTEST data set are respectively limited to $t_\mathrm{samp}U_\infty/\delta \approx 243$ and 175, owing to computational/experimental limitations. But it is worth highlighting that both these data sets are unique in the sense that τ_w as well as u, w-fluctuations (across the log region) are acquired synchronously. Consequently, in this study, we will first demonstrate consistency in the trends exhibited by the spectral estimates from all the three data sets, to confirm that differences in statistical convergence do not influence these statistics qualitatively. These spectral estimates will then be used to estimate the active and inactive components of the velocity fluctuations from the HRNBLWT data. Finally, we will analyze the synchronously acquired u, w-fluctuations from the LES

and SLTEST data to correlate the instantaneous features of their active and inactive components with τ_w-fluctuations.

In this study, we implement the spectral linear stochastic estimation (SLSE)-based decomposition methodology proposed by Deshpande *et al.* (2021) and Deshpande & Marusic (2021) to obtain the inactive component (u_{ia}) at z^+ in the log region:

$$\widetilde{u}_{\mathrm{ia}}(z^+;f^+) = H_L(z^+;f^+)\widetilde{u}_\tau(f^+), \tag{3}$$

where $\widetilde{u}_\tau(f^+) = \mathcal{F}(u_\tau^+(t^+))$ is the Fourier transform of the skin-friction-velocity fluctuation, u_τ in time (where, $u_\tau = \sqrt{\tau_w/\rho}$). The time domain equivalent of $\widetilde{u_{\mathrm{ia}}}$ is estimated simply by the inverse Fourier transform. Note that H_L in (3) corresponds to a complex-valued, scale-specific transfer kernel between the synchronously-acquired $\widetilde{u}(z)$ and $\widetilde{u_\tau}$, and is defined as:

$$H_L(z^+;T^+) = \frac{\{\widetilde{u}(z^+;T^+)\widetilde{u_\tau}^*(T^+)\}}{\{\widetilde{u_\tau}(T^+)\widetilde{u_\tau}^*(T^+)\}}. \tag{4}$$

Considering $|H_L|$ is a statistically averaged quantity, it can estimated at various z^+ in the log region for all the three multi-point data sets listed in table 1. Figure 1 depicts the absolute value of H_L at various z^+ (*i.e.*, $|H_L|(z^+)$) and compares it with the respective premultiplied spectra of U_τ. Essentially, this figure presents a visual description of both the parameters required to estimate $\widetilde{u}_{\mathrm{ia}}$ in equation (3).

The consistent variation of $|H_L|$ with increasing z^+ is evident in the low T^+ range ($\lesssim 10^4$) in figure 1 for all three data sets, confirming that inadequate statistical convergence doesn't affect the qualitative trends exhibited by LES and SLTEST data. In the highest possible T^+ range for the LES and HRNBLWT data sets, it can be noted that $|H_L|$ changes very slowly in magnitude for z^+ close to the lower-bound of the log region, and then relatively rapidly as z^+ nears the upper bound. Similar behaviour is exhibited by $|H_L|$ from the SLTEST data, z^+-range for which is predominantly close to the lower-bound of the log region ($z_l^+ \sim 2600$), thereby explaining its insignificant variation in the large T^+ range. We can thus conclude based on figure 1 that the qualitative trends exhibited by the LES and SLTEST data sets are physical and not an artefact of inadequate statistical convergence. Interested readers may refer to Deshpande *et al.* (2021) for a further detailed discussion on H_L and the full derivation of (3).

With $u_{\mathrm{ia}}(z)$ known via (3), the time series of the active component (u_a) at z can be obtained following:

$$\begin{aligned} &u_a(z^+;t^+) = u(z^+;t^+) - u_{ia}(z^+;t^+), \text{ where} \\ &u_{ia}(z^+;t^+) = \mathcal{F}^{-1}(u_{ia}(z^+;f^+)). \end{aligned} \tag{5}$$

Figure 2 demonstrates an example of implementing equations (3), (4) and (5) to obtain u_{ia} and u_{a} at the log region lower-bound ($z_l^+ \approx 2.6\sqrt{Re_\tau}$) for the HRNBLWT dataset. This plot has been adapted from Deshpande & Marusic (2021), wherein the success of this data decomposition procedure has been demonstrated previously. In figure 2, u_{a} can be noted to resemble the small-scale (high-frequency) characteristics of u, which makes sense given its association with motions localized at z^+ (active). On the other hand, u_{ia} represents large-scale variations owing to its association with taller motions. This decomposition of u permits comparison of the active ($u_a w$) and inactive ($u_{ia} w$) components of the Reynolds shear stresses with the total stress (uw) in figures 2(c,d), respectively. Here, $u_a w$ can be seen to follow the uw-signal reasonably well, while the magnitude of $u_{ia} w$ is close to zero for the majority part of the signal. This suggests that $u_a w$ is the dominant contributor to $\overline{uw}$. The result is consistent with the original description of active motions postulated by Townsend (1976), per which active motions are solely responsible for the Reynolds shear stresses. With the characteristics of active and inactive motions established based on the well-converged spectral estimates of the HRNBLWT data set, we next proceed towards implementing this same data decomposition procedure on the LES and SLTEST data.

RESULTS

Decomposition of the instantaneous velocity fluctuations from LES and SLTEST data yields synchronous u_a and u_{ia} components across the log region, which are depicted in figure 3. Figures 3(b,d) depict $u_a w$-signals (in blue shading) estimated at various z^+ for the LES and SLTEST data, respectively. These signals exhibit excellent overlap with the full Reynolds shear stress signals (uw; in black shading) at the corresponding z^+, thereby demonstrating consistency with the characteristics expected from the active motions (also exhibited previously in figure 2c by HRNBLWT data). This result reaffirms the efficacy of the SLSE-based energy decomposition scheme across a large span of Re_τ, and instills confidence in qualitative estimates from LES and SLTEST data (based on inadequately converged H_L at large T^+).

While the Reynolds shear stress (*i.e.*, active) signals are de-correlated from the τ_w-signal, the inactive signals are correlated with the τ_w-signal by definition (refer equation (3)). However, the novelty in the present analysis is revelation of the trend exhibited by synchronous u_{ia} signals across the log region. Interestingly, both the positive and negative fluctuations in the u_{ia}-signal can be seen growing in magnitude as z^+ decreases, *i.e.* with reduction in distance from the wall (indicated by an arrow). This can be associated with the increasing contributions from the attached eddy hierarchy (specifically, the inactive motions) expected with reduction in z^+. Remarkably, the τ_w-signal can be observed to be amplified close to those instants when $u_{ia} > 0$ in the log region. The entire analysis in figure 3, thus, can be deemed as a strong empirical evidence to the hypothesis of de Giovanetti *et al.* (2016), per which: "*the energy-containing motions, which essentially reside in the logarithmic and outer regions, transport the streamwise momentum to the near-wall region through their inactive part, while generating Reynolds shear stress*

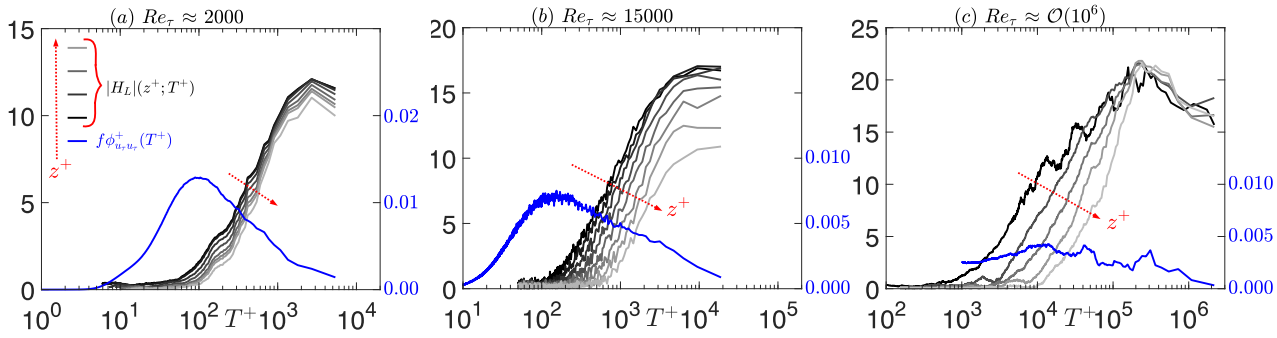

Figure 1. Modulus of the linear transfer kernel ($|H_L|(z^+;T^+)$; equation) estimated for the $Re_\tau \approx$ (a) 2000, (b) 15000 and (c) $\mathcal{O}(10^6)$ data sets. $|H_L|$ is depicted only for z^+ corresponding to the log region in the wall-normal range indicated in table 1, and its ordinate is on the primary vertical axis (left). The solid blue line represents the premultiplied spectra of the friction velocity ($f\phi^+_{u_\tau u_\tau}$), ordinate for which is on the secondary vertical axis (right).

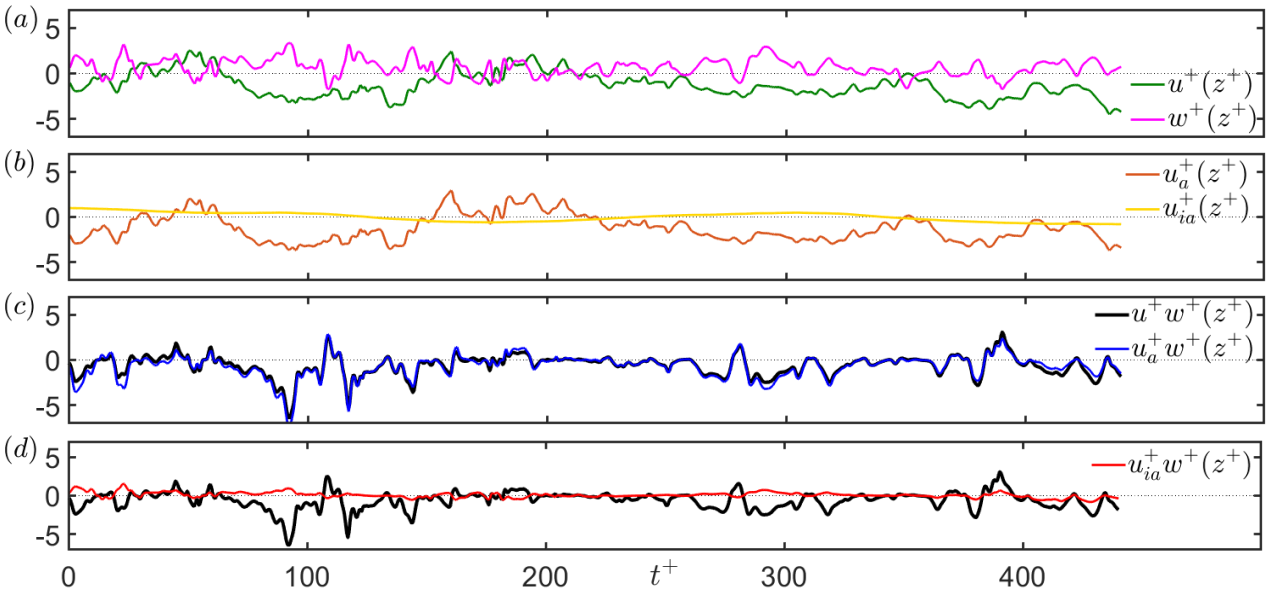

Figure 2. (a) Selected portion of synchronously acquired u- and w-time series by a cross-wire at $z^+ \approx 2.6\sqrt{Re_\tau}$ from the HRNBLWT dataset. (b) u-signal decomposed into its u_a and u_{ia} components. (c,d) Comparison of the full Reynolds shear stress (uw) signal computed from u- and w-time series in (a), with its corresponding (c) u_aw and (d) $u_{ia}w$ components.

with their wall-detached wall-normal velocity component in the region much further from the wall." Here, the 'wall-detached' part essentially refers to the active component which, as mentioned previously, is de-correlated from the wall-shear-stress signal.

SUMMARY AND CONCLUDING REMARKS

The present study implements an energy-decomposition methodology onto canonical TBL data sets, spanning a large range of Re_τ (10^3–10^6), to dissect the log-region flow into its active and inactive components. Consistent results are noted across data acquired from simulations, laboratory as well as atmospheric experiments, reaffirming the physical interpretations based on the data. Decomposition of the instantaneous velocity fluctuations unravels the unique roles played by the active and inactive components towards skin-friction drag generation, providing strong empirical evidence in support of the hypothesis of de Giovanetti *et al.* (2016). The present analysis reveals that the active motions are responsible for carrying majority of the Reynolds shear stresses (and subsequently, production of the turbulent kinetic energy) in the log region of a canonical TBL. While the inactive motions are responsible for the wall-ward transport of streamwise momentum from the log region to the wall.

The present work suggests an increased significance of the 'sweep' motions, which correspond to the fourth quadrant of the Reynolds shear stresses: $u > 0$, $w < 0$, in the log region of high Re_τ TBLs. Interestingly, recent explainable deep learning models trained on canonical TBL data sets (Cremades *et al.*, 2024) have identified these sweeps amongst the most dynamically significant coherent motions in high Re_τ wall turbulence. While the growing statistical significance of sweeps has previously been quanti-

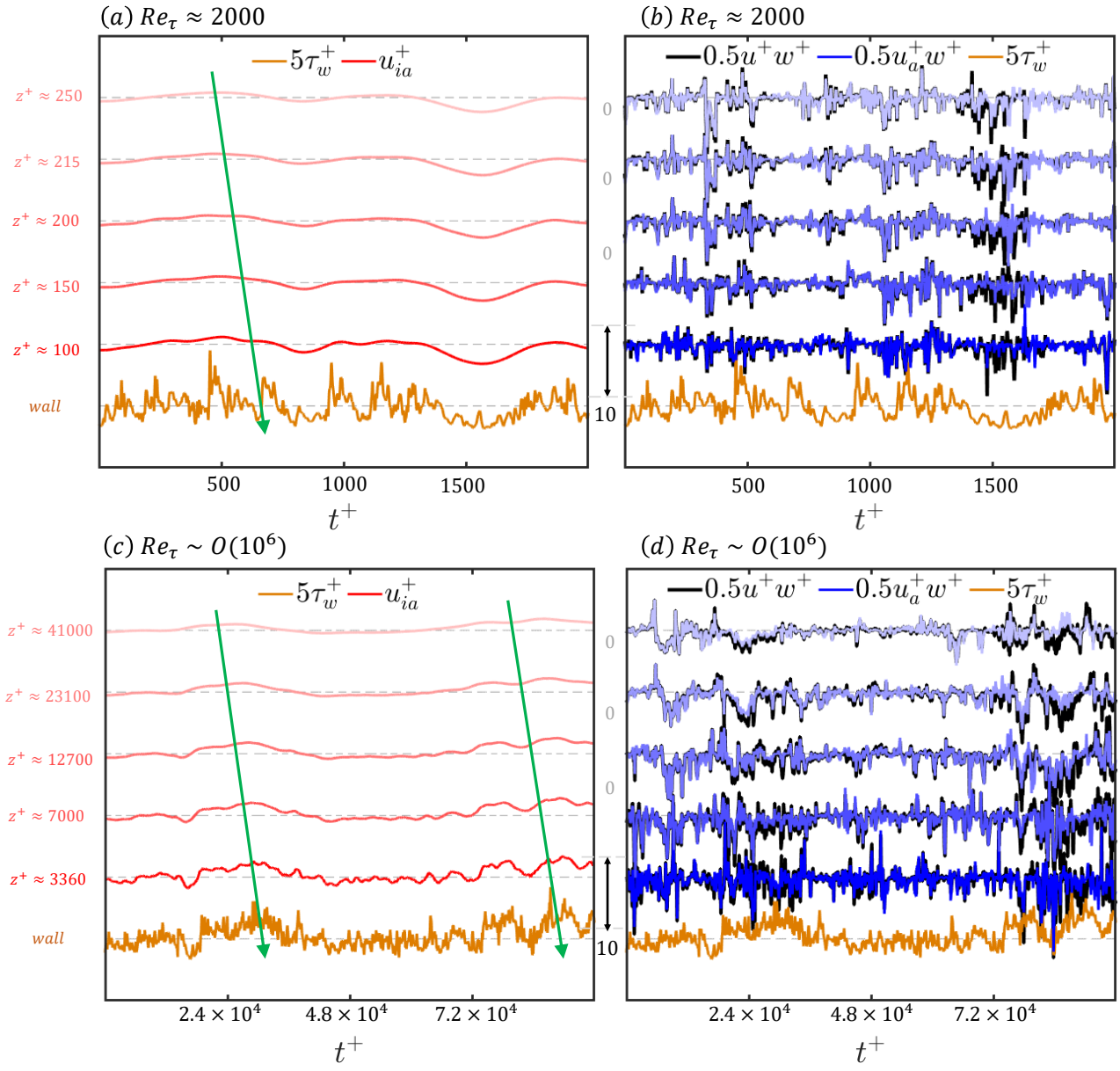

Figure 3. (a,c) Portion of the u_{ia}-signal estimated at various z^+, in the log region, from the (a) LES and (c) SLTEST datasets. (b,d) Portion of the $u_a w$-signal corresponding to the same time instants and z^+ as in (a,c), compared with the uw-signal at the respective z^+ for the (b) LES and (d) SLTEST datasets. Dark to light shading for these signals indicates increase in z^+, with each signal offset vertically as highlighted. Green arrows in (a,c) are used to suggest the transfer of streamwise momentum from the log region towards the wall, with the latter represented by the τ_w-signal.

fied in high-Re_τ experiments (Deshpande & Marusic, 2021), more detailed work is currently in progress to demonstrate their important role in the energy transfer mechanisms of the outer region of TBLs. Another interesting line of future research could be towards investigating the relationship (if any) between Townsend's active and inactive motions, with the dynamically 'important' coherent structures identified by explainable deep learning models (Cremades *et al.*, 2024). Besides the aforementioned developments associated with our fundamental understanding, the present work also carries the potential to inform the design of future energy-efficient flow-control strategies.

ACKOWLEDGEMENTS

R. D. is supported by University of Melbourne's Postdoctoral Fellowship. Funding is gratefully acknowledged from ONR: N62909-23-1-2068 (R.D., I.M.), and to R.V. from ERC grant no. '2021-CoG-101043998, DEEPCONTROL'.

REFERENCES

Corke, T. C. & Thomas, F. O. 2018 Active and passive turbulent boundary-layer drag reduction. *AIAA journal* **56** (10), 3835–3847.

Cremades, A., Hoyas, S., Deshpande, R., Quintero, P., Lellep, M., Lee, W. J., Monty, J., Hutchins, N., Linkmann, M., Marusic, I. & Vin-

uesa, R. 2024 Identifying regions of importance in wall-bounded turbulence through explainable deep learning. *Accepted in Nat. Comm. [arXiv preprint arXiv:2302.01250]* .

Deck, S., Renard, N., Laraufie, R. & Weiss, P. 2014 Large-scale contribution to mean wall shear stress in high-Reynolds-number flat-plate boundary layers up to 13650. *J. Fluid Mech.* **743**, 202–248.

Deshpande, R. & Marusic, I. 2021 Characterising Momentum Flux Events in High Reynolds Number Turbulent Boundary Layers. *Fluids* **6** (4), 168.

Deshpande, R., Monty, J. P. & Marusic, I. 2021 Active and inactive components of the streamwise velocity in wall-bounded turbulence. *Journal of Fluid Mechanics* **914**, A5.

Eitel-Amor, G., Örlü, R. & Schlatter, P. 2014 Simulation and validation of a spatially evolving turbulent boundary layer up to Re_θ= 8300. *Int. J. Heat Fluid Flow* **47**, 57–69.

de Giovanetti, M., Hwang, Y. & Choi, H. 2016 Skin-friction generation by attached eddies in turbulent channel flow. *Journal of Fluid Mechanics* **808**.

Hultmark, M., Vallikivi, M., Bailey, S. C. C. & Smits, A. J. 2012 Turbulent pipe flow at extreme Reynolds numbers. *Phys. Rev. Lett.* **108** (9), 094501.

Jimenez, J. & Hoyas, S. 2008 Turbulent fluctuations above the buffer layer of wall-bounded flows. *J. Fluid Mech.* **611**, 215–236.

Kim, J. 2011 Physics and control of wall turbulence for drag reduction. *Phil. Trans. R. Soc. A* **369** (1940), 1396–1411.

Lee, M. & Moser, R. D. 2015 Direct numerical simulation of turbulent channel flow up to $Re_\tau \approx 5200$. *J. Fluid Mech.* **774**, 395–415.

Marusic, I., Chandran, D., Rouhi, A., Fu, M. K., Wine, D., Holloway, B., Chung, D. & Smits, A. J. 2021 An energy-efficient pathway to turbulent drag reduction. *Nat. Commun.* **12** (1), 1–8.

Marusic, I. & Heuer, W. D. C. 2007 Reynolds number invariance of the structure inclination angle in wall turbulence. *Physical review letters* **99** (11), 114504.

Marusic, I., Mathis, R. & Hutchins, N. 2010 High Reynolds number effects in wall turbulence. *Int. J. Heat Fluid Flow* **31** (3), 418–428.

Marusic, I. & Monty, J. P. 2019 Attached eddy model of wall turbulence. *Annual Review of Fluid Mechanics* **51**, 49–74.

Panton, R. L. 2007 Composite asymptotic expansions and scaling wall turbulence. *Philosophical Transactions of the Royal Society A: Mathematical, Physical and Engineering Sciences* **365** (1852), 733–754.

Pirozzoli, S., Romero, J., Fatica, M., Verzicco, R. & Orlandi, P. 2021 One-point statistics for turbulent pipe flow up to $Re_\tau \approx 6000$. *J. Fluid Mech.* **926**, A28.

Smits, A.J., McKeon, B.J. & Marusic, I. 2011 High–Reynolds number wall turbulence. *Annu. Rev. Fluid Mech.* **43**.

Talluru, K. M., Baidya, R., Hutchins, N. & Marusic, I. 2014 Amplitude modulation of all three velocity components in turbulent boundary layers. *Journal of Fluid Mechanics* **746**, R1.

Townsend, A.A. 1976 *The structure of turbulent shear flow*, 2nd edn. Cambridge University Press.